

A double molecular disc in the triple-barred starburst galaxy NGC 6946: structure and stability

Alessandro B. Romeo^{1*} and Kambiz Fathi^{2,3}

¹*Department of Earth and Space Sciences, Chalmers University of Technology, SE-41296 Gothenburg, Sweden*

²*Department of Astronomy, Stockholm University, AlbaNova Centre, SE-10691 Stockholm, Sweden*

³*Oskar Klein Centre for Cosmoparticle Physics, Stockholm University, SE-10691 Stockholm, Sweden*

Accepted 2015 May 28. Received 2015 May 22; in original form 2015 March 04

ABSTRACT

The late-type spiral galaxy NGC 6946 is a prime example of molecular gas dynamics driven by ‘bars within bars’. Here we use data from the BIMA SONG and HERACLES surveys to analyse the structure and stability of its molecular disc. Our radial profiles exhibit a clear transition at distance $R \sim 1$ kpc from the galaxy centre. In particular, the surface density profile breaks at $R \approx 0.8$ kpc and is well fitted by a double exponential distribution with scale lengths $R_1 \approx 200$ pc and $R_2 \approx 3$ kpc, while the 1D velocity dispersion σ decreases steeply in the central kpc and is approximately constant at larger radii. The fact that we derive and use the full radial profile of σ rather than a constant value is perhaps the most novel feature of our stability analysis. We show that the profile of the Q stability parameter traced by CO emission is remarkably flat and well above unity, while the characteristic instability wavelength exhibits clear signatures of the nuclear starburst and inner bar within bar. We also show that CO-dark molecular gas, stars and other factors can play a significant role in the stability scenario of NGC 6946. Our results provide strong evidence that gravitational instability, radial inflow and disc heating have driven the formation of the inner structures and the dynamics of molecular gas in the central kpc.

Key words: instabilities – ISM: kinematics and dynamics – galaxies: individual: NGC 6946 – galaxies: ISM – galaxies: kinematics and dynamics – galaxies: structure.

1 INTRODUCTION

Non-axisymmetric galactic structures such as bars and spiral arms contain a significant fraction of the disc material, and thus have a prominent role in the evolution of their host galaxies (e.g., Lindblad 1960). Such structures are efficient drivers for the redistribution of angular momentum, and induce strong flows and streaming motions in their hosts (e.g., Schwarz 1984). The interstellar gas is highly inhomogeneous and prone to gravitational instability, thermal instability and turbulent compression (see, e.g., Mac Low & Klessen 2004). When large-scale flows converge, molecular clouds can form rapidly in regions dense enough to form H_2 (e.g., Glover & Mac Low 2007; Tasker 2011). Galactic-scale flows also pump turbulent energy into the rotating gas disc, which in turn initiates local instabilities (e.g., Renaud et al. 2013) and produces further heating of the disc (e.g., Martig et al. 2014). A thorough understanding of such multi-scale processes requires a detailed analysis of the structures that originate from them. Galaxies hosting a hierarchy of inter-

linked non-axisymmetric structures are thus especially suitable for analysing disc instability and its effects on structure formation and evolution.

The late-type spiral galaxy NGC 6946 is a prime example of such dynamics: it hosts an outer bar that drives the evolution of structure in the disc, from its prominent spiral arms to an inner bar within bar feeding a nuclear starburst (e.g., Elmegreen et al. 1992; Schinnerer et al. 2006; Fathi et al. 2007; Tsai et al. 2013). The gravitational instability of NGC 6946 has been investigated in several works, most often in the context of large galaxy surveys (e.g., Kennicutt 1989; Ferguson et al. 1998; Fuchs & von Linden 1998; Martin & Kennicutt 2001; Leroy et al. 2008; Romeo & Wiegert 2011; Hoffmann & Romeo 2012; Romeo & Falstad 2013). Ferguson et al. (1998) showed how sensitive the results are to the gas 1D velocity dispersion σ_g : assuming that $\sigma_g = 6 \text{ km s}^{-1}$, the value proposed by Kennicutt (1989), NGC 6946 turns out to be unstable up to the edge of the optical disc, while using a radial profile of σ_g derived from observations yields stability across the entire disc! Martin & Kennicutt (2001) pointed out that radial variation in σ_g remains controversial because such measurements demand both high angular

* E-mail: romeo@chalmers.se

resolution and high brightness sensitivity, requirements not met by most observations. Fortunately, recent CO and H I galaxy surveys (BIMA SONG, HERACLES and THINGS) have provided high-quality measurements of gas kinematics, which allow deriving reliable radial profiles of σ_g (e.g., Caldú-Primo et al. 2013).

Another source of concern in this stability context is the multi-component (gas+stars) nature of the disc. Unfortunately, there are no stellar spectra available for NGC 6946, i.e. we have no information about the stellar radial velocity dispersion σ_* . Romeo & Falstad (2013) used a model-based radial profile of σ_* , originally proposed by Leroy et al. (2008), and analysed the stability of NGC 6946 together with other spirals from The H I Nearby Galaxy Survey (THINGS). They showed that NGC 6946 is unstable only within the central kpc, and that molecular gas (H_2) is the main driver of instability if σ_{H_2} is within the range of values used in previous investigations, i.e. 6 km s^{-1} (e.g., Kennicutt 1989; Wilson et al. 2011) to 11 km s^{-1} (e.g., Leroy et al. 2008). They also found that if $\sigma_{H_2} \approx 6 \text{ km s}^{-1}$, then molecular gas controls the local stability level of the disc up to about 5 kpc from the centre. Stars dominate the value of the Q stability parameter at larger distances, while atomic gas has a negligible effect up to the optical radius.

The multi-component stability analysis of Romeo & Falstad (2013) has one main limitation: it uses observationally motivated values of σ_{H_2} , rather than a radial profile $\sigma_{H_2}(R)$ derived from observations. This is a serious limitation because, as discussed above, molecular gas plays a primary role even beyond the central kpc, and up to a radius R_{max} that depends on σ_{H_2} : $R_{\text{max}} \approx 5 \text{ kpc}$ for $\sigma_{H_2} \approx 6 \text{ km s}^{-1}$; the larger σ_{H_2} , the smaller R_{max} . This illustrates how important it would be to have a reliable radial profile of σ_{H_2} up to $R \approx 5 \text{ kpc}$, and suggests that a one-component stability analysis based on such a profile could be a proper starting point for discussing the roles that stars, the various gas phases, the various bar structures and other components play in the stability scenario of NGC 6946.

In this paper, we analyse NGC 6946 focusing on the structure and stability of its molecular disc. For this purpose, we derive high-quality radial profiles of the surface density, 1D velocity dispersion and epicyclic frequency up to $R = 5 \text{ kpc}$, using data from two recent surveys: the BIMA Survey of Nearby Galaxies (BIMA SONG, Helfer et al. 2003), and the HERA CO-Line Extragalactic Survey (HERACLES, Leroy et al. 2009). We also analyse the link between structure formation and gravitational instability in the central kpc, and discuss the roles that CO-dark molecular gas, stars and other factors play in the stability scenario of NGC 6946.

2 NGC 6946

NGC 6946 is a low-inclination grand-design barred spiral galaxy with an observed axis ratio of 0.87 (Carignan et al. 1990; Zimmer et al. 2004; Boomsma 2007). We adopt a distance of 5.9 Mpc (Leroy et al. 2009), so that $1''$ corresponds to 28.6 pc. Numerous morphological and kinematic studies by e.g. Elmegreen et al. (1992), Regan & Vogel (1995), Elmegreen et al. (1998), Kennicutt et al. (2003), Schinnerer et al. (2006) and Fathi et al. (2007) have revealed clear sig-

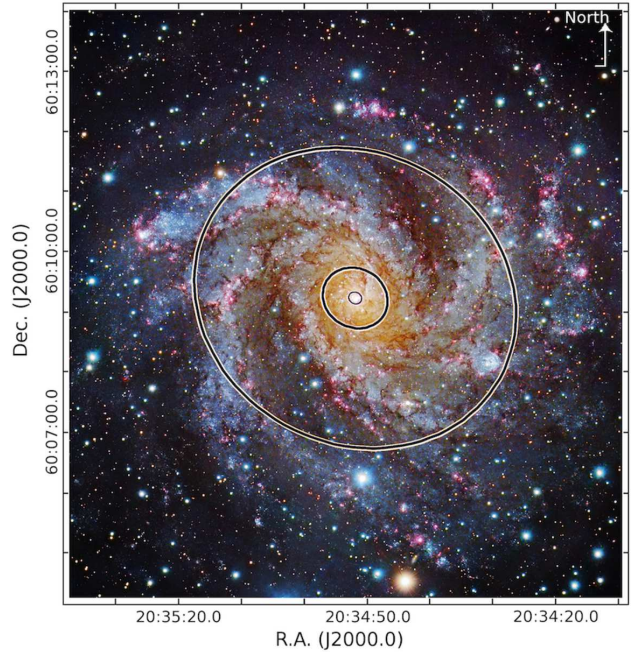


Figure 1. A composite *BVI* image of NGC 6946, with the North-East direction displayed in the top-right corner. The three ellipses show the outermost radius of the analysis presented here (5 kpc), and the approximate radii of the inner bar within bar (1 kpc and 200 pc). The ellipses take into account the inclination and position angle of the galaxy. Note how the dust lane near the centre in the North direction changes angle at the 1 kpc radius, i.e. approximately where the oILR of the outer bar is located. Image courtesy of Subaru Telescope (NAOJ) and Robert Gendler.

natures of three main gravitational distortions: a large but weak bar-like structure with a projected ellipticity of 0.25 and radius $R \approx 4.5'$, a secondary bar with radius $R \approx 60''$, and a nuclear bar with ellipticity 0.4 and radius $R \approx 8''$. Fathi et al. (2007, 2009) found that the pattern speed of the weak outermost bar is $\Omega_p = 25 \pm 6 \text{ km s}^{-1} \text{ kpc}^{-1}$, and used this value to place the corotation radius between $250''$ and $300''$, the outer inner Lindblad resonance (oILR) radius between $30''$ and $60''$, and the inner inner Lindblad resonance (iILR) radius below $15''$. In addition, direct measurements of the pattern speed of the secondary bar showed that this lies in the range $39 \pm 8 \text{ km s}^{-1} \text{ kpc}^{-1}$ (Zimmer et al. 2004), $47^{+3}_{-2} \text{ km s}^{-1} \text{ kpc}^{-1}$ (Fathi et al. 2007), and $51 \pm 3 \text{ km s}^{-1} \text{ kpc}^{-1}$ (Font et al. 2014).

These dynamical and structural properties agree well with those found by Schinnerer et al. (2006, 2007), and converge towards a scenario where the outer bar drives the evolution of structure in NGC 6946 (see Fig. 1): the secondary bar is within the oILR of the outer bar, while the nuclear bar is within the iILR of the outer bar and has approximately the same radial extent as the nuclear starburst ($R \approx 5.5''$; Schinnerer et al. 2006). Such structural interplay is indeed interesting from a dynamical point of view, and makes NGC 6946 an ideal laboratory for a detailed analysis of its disc structure and stability.

3 DATA AND METHOD

3.1 Molecular gas data

In this work we analyse the molecular gas content and kinematics of NGC 6946 as traced by the CO $J(1 \rightarrow 0)$ and CO $J(2 \rightarrow 1)$ lines, and based on archival single-dish and interferometric observations from the BIMA SONG (Helfer et al. 2003) and HERACLES (Leroy et al. 2009) surveys, respectively. We have retrieved the reduced data cubes from the archives made available by these teams. All the details concerning data acquisition, data reduction and data quality are presented in the two papers above (see also Leroy et al. 2008 for the HERACLES data). Most important for our analysis is that the spatial resolution of the CO $J(1 \rightarrow 0)$ data is approximately $5'' \times 6''$, sampled at $1''/\text{pix}$ and with a channel width of 10 km s^{-1} . The CO $J(2 \rightarrow 1)$ data have a spatial resolution of approximately $11''$, sampled at $2''/\text{pix}$ and with a channel width of 5.2 km s^{-1} .

To derive the molecular gas surface density (Σ), line-of-sight velocity (V_{los}) and velocity dispersion (σ), we use two methods in parallel, namely calculating the moment maps and applying Gaussian fits to the individual spectra. We find a good agreement between the moment maps and the results of Gaussian fitting. We also find that our amplitude maps match the zeroth-moment maps presented by the BIMA SONG and HERACLES teams. One advantage of applying Gaussian fits is that we can get better covering maps if we use a Hanning smoothing algorithm in the spectral direction before fitting the individual Gaussian profiles (e.g., Hernandez et al. 2005; Daigle et al. 2006). This procedure does not affect the line amplitude or shift. However, it artificially broadens the individual spectra by $\Delta\sigma \approx 4.4 \text{ km s}^{-1}$, which we then subtract quadratically from the derived velocity dispersion maps. Finally, we apply a cleaning procedure by removing all the spectra for which the emission line amplitude is smaller than twice the rms noise, σ is smaller than half the velocity channel, and the formal error in the derived σ is greater than 10 km s^{-1} .

A careful inspection of the individual spectra reveals the presence of multiple components at different locations (mostly in the central few 100 pc). In view of the good agreement between the moment maps and the single-Gaussian fits, and in view of the complications involved in multiple-profile fitting schemes (Blasco-Herrera et al. 2010), we do not use profile decomposition methods. All subsequent analysis is thus based on single-Gaussian profile fitting.

3.2 Radial profiles by means of robust statistics

We derive the radial profiles of Σ and σ using robust statistics, which are especially useful when the data contain a significant fraction of outliers (see, e.g., Rousseeuw 1991; Müller 2000; Huber & Ronchetti 2009; Feigelson & Babu 2012). This is indeed the case for the Σ and σ maps, where a non-negligible number of pixel values (e.g. those associated with H II regions) deviate strongly from a normal distribution. To derive the radial profiles of Σ and σ , we divide their maps into tilted rings, which are circular in the plane of the galaxy, and compute the median values of Σ and σ in each ring. We then estimate the uncertainty in these median values via the median absolute deviation (MAD):

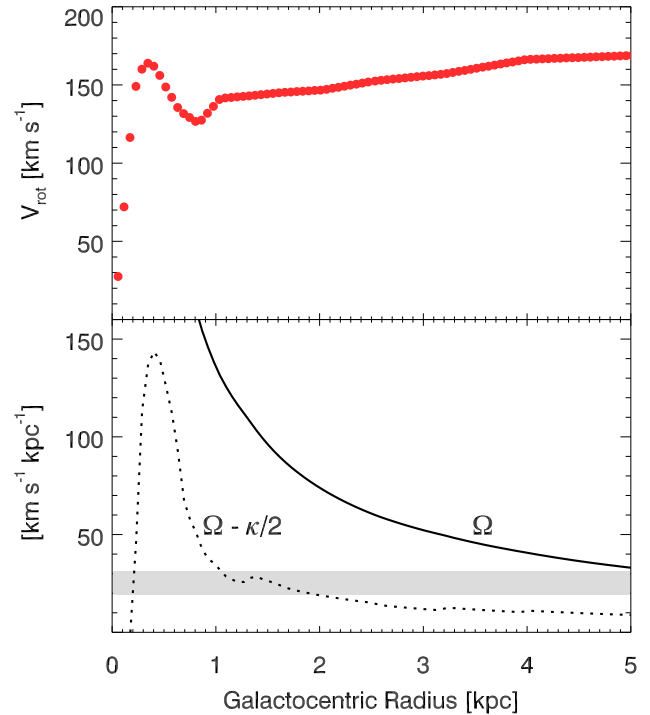


Figure 2. The rotation curve (top) and frequency diagram (bottom) of NGC 6946. Adopting a pattern speed of $25 \pm 6 \text{ km s}^{-1} \text{ kpc}^{-1}$ for the weak outer bar (Fathi et al. 2009), we recover resonance radii consistent with the literature. The rotation curve is consistent with measurements based on different molecules, neutral atomic and ionized gas. The frequency diagram is based on smoothed curves so as to mimic the resolution of the curves presented in the literature (see Sect. 2).

$$\Delta X_{\text{med}} = 1.858 \times \text{MAD} / \sqrt{N}, \quad (1)$$

$$\text{MAD} = \text{median}\{|X_i - X_{\text{med}}|\}, \quad (2)$$

where X_i are the individual measurements of Σ or σ , X_{med} is their median value, and N is the number of resolution elements in each ring (i.e. the number of pixels in the ring divided by the number of pixels per resolution element). Eqs (1) and (2) are the robust counterparts of the formula traditionally used for estimating the uncertainty in the mean: $\Delta X_{\text{mean}} = \text{SD} / \sqrt{N}$, where SD denotes the standard deviation (see again Müller 2000). Indeed, the median and the median absolute deviation provide robust statistical estimates of the ‘central value’ and the ‘width’ of a data set, respectively, even when almost 50% of the data are outliers!

Our numerous tests with varying ring radii and widths confirm that the high quality of the BIMA SONG and HERACLES data allow a derivation of Σ and σ at radii smaller than the synthesized beam size of the interferometric observations. This is mainly thanks to the good sampling of the resolution element. The smallest reliable step is found to be $2''$, which corresponds to 57 pc. This is the step size adopted throughout our analysis. The inner 2.5 kpc of the Σ and σ profiles presented here are derived from the BIMA SONG data, while the profiles at larger radii are derived from the HERACLES data. The H_2 surface density is converted to physical units by adopting an X_{CO} conversion factor of $2 \times 10^{20} \text{ cm}^{-2} (\text{K km s}^{-1})^{-1}$, consistent with Leroy et al. (2008) and Donovan Meyer et al. (2012). We also correct

for the contribution of Helium multiplying by a factor of 1.36. To further match the BIMA SONG and HERACLES data, we use $\text{CO } J(2 \rightarrow 1)/\text{CO } J(1 \rightarrow 0) = 0.8$, as in Leroy et al. (2008).

In addition to the Σ and σ profiles, a stability analysis also requires the epicyclic frequency κ at each radius, which we derive from the observed rotation curve. To calculate the rotation curve, we assume that circular rotation is the dominant kinematic feature, and that our measurements refer to positions on a single inclined disc. We then use the tilted ring method combined with the harmonic decomposition formalism (e.g., Schoenmakers et al. 1997; Wong et al. 2004; Fathi et al. 2005). Given that this procedure involves fitting several parameters at each radius of the observed velocity field (contrary to simply finding the median values of Σ and σ), we cannot use the same initial step size. Hence we apply a larger radial step, and interpolate linearly to obtain the rotation curve at all radii where we have calculated the robust Σ and σ values. Here the cut in the data is made at a radius of 0.7 kpc. Once the rotation curve V_{rot} is calculated at each radius R , we derive the angular frequency $\Omega = V_{\text{rot}}/R$ and the epicyclic frequency $\kappa = \sqrt{R d\Omega^2/dR + 4\Omega^2}$. Setting up the standard frequency diagram (see Fig. 2), we confirm the location of the inner Lindblad resonances of the weak outer bar discussed in Sect. 2.

4 RESULTS

4.1 Structure of the disc

Fig. 3 illustrates that the radial profiles of the epicyclic frequency, κ , 1D velocity dispersion, σ , and surface density, Σ , break at $R \sim 1$ kpc. This tells us that the inner region of NGC 6946 is physically distinct from the rest of the disc, and that radial inflow (increase of Σ and κ towards the centre) and disc heating (increase of σ towards the centre) have both played a primary role in shaping the central kpc. This is consistent with the fact that the dynamics of NGC 6946 is driven by three bars, and that the strong secondary bar extends up to $R \sim 1$ kpc (see Sect. 2). Since bars are non-axisymmetric gravitational instabilities, they exert torques on the disc, which transport angular momentum and energy outwards, leading to the two processes mentioned above: radial inflow and disc heating¹ (e.g., Zhang 1998; Griv et al. 2002; Romeo et al. 2003, 2004; Fathi et al. 2008; Agertz et al. 2009; Krumholz & Burkert 2010; Forbes et al. 2012, 2014). Besides, bars within bars make such processes highly efficient (e.g., Shlosman et al. 1989; Friedli & Martinet 1993; Rautiainen et al. 2002; Shlosman 2002). A dynamically cool inner disc and especially nuclear star formation make such structures long-lived, even in the absence of mode coupling (Du et al. 2015; Wozniak 2015).

¹ Disc heating is a natural consequence of radial inflow and is mediated by local gravitational instabilities. Although there are still open questions, the basic idea behind this process is simple, and is beautifully illustrated in sect. 7.1 of Kormendy & Kennicutt (2004). Radial inflow increases both Σ and κ , but Σ ‘wins’ and the Toomre (1964) parameter $Q = \kappa\sigma/\pi G\Sigma$ decreases. As Q drops below a critical value of order unity, local gravitational instabilities set in and increase σ , thus heating the disc.

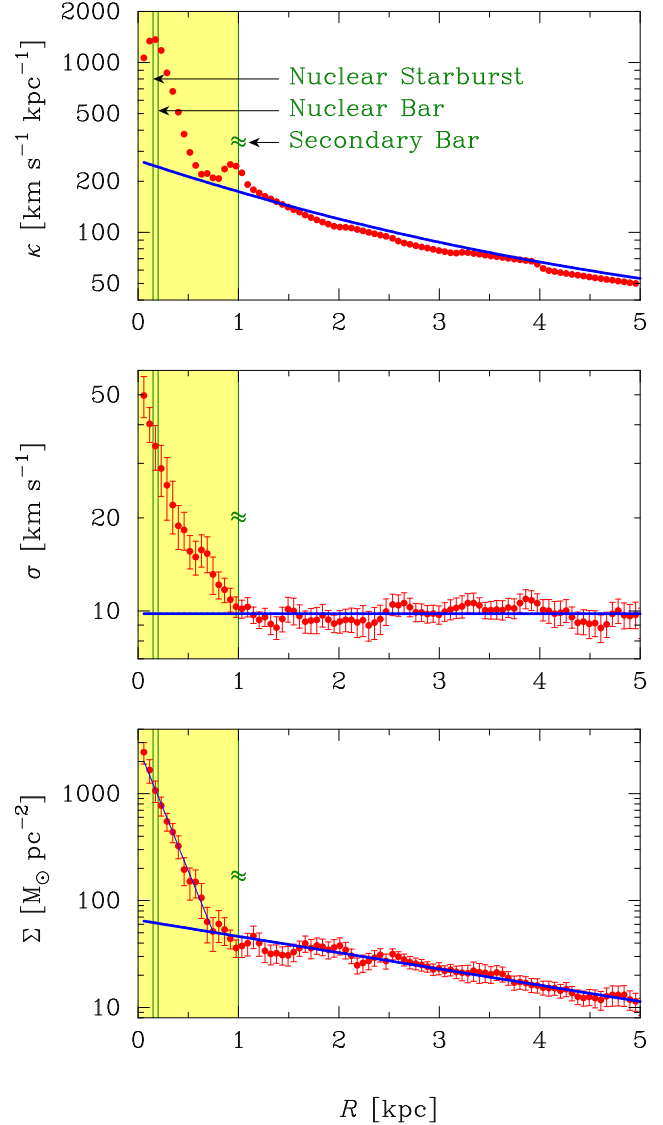


Figure 3. Radial profiles of the epicyclic frequency (top), 1D velocity dispersion (middle) and surface density (bottom) of molecular gas in NGC 6946. The thick lines are fits to these profiles over the radial range 1–5 kpc, extrapolated into the central kpc. The thin lines represent the approximate radial extent of the nuclear starburst and inner bar within bar. The bottom panel also shows a robust, median-based, exponential fit to $\Sigma(R)$ for $R \leq 0.8$ kpc.

Look now at the thick lines in Fig. 3. These are simple but accurate fits to the radial profiles of κ , σ and Σ for $1 \text{ kpc} \leq R \leq 5 \text{ kpc}$.

(i) $\kappa_{\text{fit}}(R)$ is the fit originally proposed by Leroy et al. (2008); see their eqs (13) and (B1), and table 4.

(ii) $\sigma_{\text{fit}}(R) \simeq 10 \text{ km s}^{-1}$ is the median of the 1D velocity dispersion data. This value is comparable to those found by Walsh et al. (2002) and Caldú-Primo et al. (2013) for $R \gtrsim 2 \text{ kpc}$.

(iii) $\Sigma_{\text{fit}}(R) = \Sigma_2 e^{-R/R_2}$, with $\Sigma_2 \simeq 66 \text{ M}_\odot \text{ pc}^{-2}$ and $R_2 \simeq 2.9 \text{ kpc}$, is a median-based fit to the surface density data. The disc scale length R_2 is 50% larger than that found by Leroy et al. (2008, 2009). Note, however, that they fitted an exponential function to the whole molecular disc, i.e.

they included the central kpc, which we have shown to be physically distinct from the rest of the disc.

Extrapolating these fits back to $R < 1$ kpc allows us to predict how the inner region of NGC 6946 differs dynamically from the rest of the disc. In particular, we have compelling evidence that the nuclear disc is also exponential. A robust, median-based, fit to the radial profile of Σ for $R \leq 0.8$ kpc yields: $\Sigma_{\text{FIT}}(R) = \Sigma_1 e^{-R/R_1}$, with $\Sigma_1 \simeq 2700 \text{ M}_\odot \text{ pc}^{-2}$ and $R_1 \simeq 190 \text{ pc}$. This is also the approximate radial extent of the nuclear bar (see Sect. 2). The precise radius at which the surface density breaks is $R_{\text{break}} \simeq 0.75$ kpc, and the corresponding density is $\Sigma_{\text{break}} \simeq 50 \text{ M}_\odot \text{ pc}^{-2}$. This means that the nuclear molecular disc extends over four exponential scale lengths, thus actually more than the main molecular disc!

Our results concerning the nuclear molecular disc of NGC 6946 should be compared with those of Regan et al. (2001). They showed that the radial profile of CO surface brightness decreases steeply for $R \lesssim 1.5$ kpc, then increases inside a transition layer of radial width $\Delta R \approx 1$ kpc, and finally decreases again (see their fig. 2). They concluded that the CO emission excess in the central kpc looks like a bulge, while the decrease at larger radii corresponds to an exponential disc. This is in contrast to our findings. We have shown that the CO surface density excess in the central kpc is indeed a nuclear exponential disc, and that the transition from the nuclear to the main disc is sharp: the slope of $\Sigma(R)$ changes abruptly across the radius $R_{\text{break}} \simeq 0.75$ kpc. In addition, the fact that the central 1D velocity dispersion is very high, $\sigma_0 \approx 50 \text{ km s}^{-1}$, does not tell us that the nuclear structure is bulge-like, given that the central surface density is as large as $\Sigma_0 \approx 2500 \text{ M}_\odot \text{ pc}^{-2}$. A real upper limit on the central disc scale height can be estimated by neglecting the gravity of the stellar disc, and by assuming that the molecular disc is self-gravitating and isothermal along the vertical direction: $h_0 \ll \sigma_0^2 / \pi G \Sigma_0 \approx 70\text{--}80 \text{ pc}$ (other assumptions would only modify our estimate by a factor of order unity; see, e.g., van der Kruit & Freeman 2011). Since the nuclear disc has scale length $R_1 \simeq 190 \text{ pc}$ and extends up to $R_{\text{break}} \simeq 0.75$ kpc, we find that $h_0 \ll 0.4 R_1 \approx 0.1 R_{\text{break}}$. Thus the central 1D velocity dispersion is consistent with a nuclear molecular disc of moderate thickness.

Note that $\sigma_0 \approx 50 \text{ km s}^{-1}$ is comparable to the CO values found by Schinnerer et al. (2006) and to the central stellar velocity dispersions measured by Engelbracht et al. (1996), Ho et al. (2009) and Kormendy et al. (2010). Note also that $R_2 \approx 3$ kpc is comparable to the scale length of the stellar disc found by Kormendy et al. (2010), and that $R_1/R_2 \approx 0.07$ is within the range of pseudobulge-to-disc scale length ratios observed in spiral galaxies (e.g., Courteau et al. 1996; MacArthur et al. 2003; Fisher & Drory 2008). As noted by John Kormendy (private communication), these results are consistent with the predictions of the general evolution picture reviewed in Kormendy & Kennicutt (2004) and Kormendy (2013).

4.2 Stability of the disc

Fig. 4 shows the radial profiles of two useful stability diagnostics. One is the Toomre-like parameter

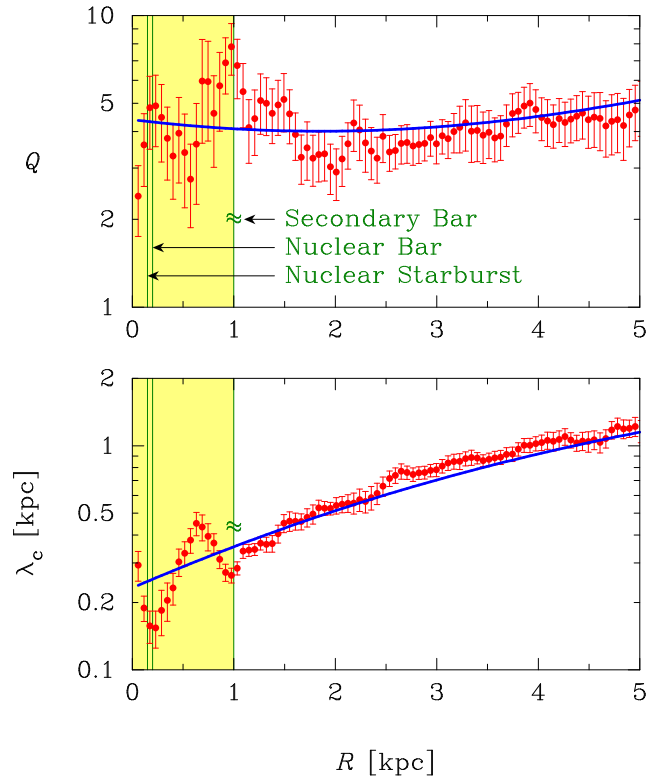


Figure 4. Radial profiles of the Q stability parameter (top) and characteristic instability wavelength (bottom) for molecular gas in NGC 6946. The thick lines are predictions based on the fits to $\kappa(R)$, $\sigma(R)$ and $\Sigma(R)$ shown in Fig. 3. The thin lines represent the approximate radial extent of the nuclear starburst and inner bar within bar.

$$Q = \frac{3}{2} \frac{\kappa \sigma}{\pi G \Sigma}, \quad (3)$$

which measures the stability level of realistically thick gas discs (see Romeo & Falstad 2013).² The other is the characteristic instability wavelength,

$$\lambda_c = 2\pi \frac{\sigma}{\kappa}, \quad (4)$$

i.e. the scale at which the disc becomes locally unstable as Q drops below unity (see again Romeo & Falstad 2013). Fig. 4 also shows $Q_{\text{fit}}(R)$ and $\lambda_{c \text{ fit}}(R)$, which are predictions based on the fits to the radial profiles of κ , σ and Σ (thick lines).

The top panel of Fig. 4 illustrates that $Q(R)$ is fairly constant for $R \gtrsim 1$ kpc, while it varies significantly for $R \lesssim 1$ kpc. This is not surprising since the central kpc is the region where $\kappa(R)$, $\sigma(R)$ and $\Sigma(R)$ vary most. As we move towards the centre, κ and σ increase by a factor of 5–7, while Σ increases by two orders of magnitude (see Fig. 3). What is surprising is that, in spite of such strong variations, $Q(R)$ fluctuates around a constant value, deviating from it by less than a factor of two! What drives the radial variation of Q in the central kpc? We will clarify this point in Sect. 5.1. Here instead we focus on the overall flatness of $Q(R)$, which is an eloquent example of self-regulation:

² We have assumed that the velocity dispersion is isotropic ($\sigma_z = \sigma_R$). This is justified by the fact that interstellar gas can, to first approximation, be regarded as a collisional component.

the disc of NGC 6946 is driven by processes that keep it at a fairly constant stability level, except in the central kpc, where the value of Q is modulated by the nuclear starburst and inner bar within bar. Current dynamical models of star-forming galaxies suggest that such self-regulation processes are determined by a balance among gravitational instability, star formation and accretion (e.g., Bertin & Romeo 1988; Romeo 1990; Agertz et al. 2009; Krumholz & Burkert 2010; Elmegreen 2011; Cacciato et al. 2012; Forbes et al. 2012, 2014). According to these models, galactic discs should (i) have a constant stability level, and (ii) be close to marginal instability. The results illustrated above are clearly consistent with point (i), while the fact that the Q stability parameter is well above unity ($Q_{\text{fit}} = 4\text{--}5$) seems to tell us that the disc of NGC 6946 is fairly far from marginal instability. Is Q really so large? This is a complex issue that we will discuss in Sect. 5.2.

Our results concerning $Q(R)$ seem comparable to those of Romeo & Falstad (2013), who showed that the stability level of THINGS spirals is, on average, remarkably flat and well above unity (see their figs 4 and 5). Note, however, that those results cannot be directly compared with ours because they concern the THINGS sample as a whole, not each of the spirals or in particular NGC 6946.

The bottom panel of Fig. 4 illustrates that $\lambda_c(R)$ increases monotonically for $R \gtrsim 1$ kpc, while it has two well-defined minima for $R \lesssim 1$ kpc. The location of such minima is strongly correlated with the radial extent of the three structures in the central kpc: the nuclear starburst (NS), the nuclear bar (NB) and the secondary bar (SB). We find that:

$$R_{\text{min1}} \approx 150\text{--}200 \text{ pc} \approx R_{\text{NS}}, R_{\text{NB}}; \quad (5)$$

$$R_{\text{min2}} \approx 1 \text{ kpc} \approx R_{\text{SB}}. \quad (6)$$

This is surprising because $\lambda_c(R)$ is meant to be a diagnostic for characterizing *local* gravitational instabilities (such as those associated with star-forming rings, complexes/clumps and starbursts), and not *global* gravitational instabilities (such as those classically associated with the formation of spiral and bar structures). Thus Eqs (5) and (6) point out $\lambda_c(R)$ as a powerful diagnostic, which accurately predicts the sizes of starbursts and bars within bars. In contrast, remember that $Q(R)$ is only modulated by such structures. What drives the radial variation of λ_c in the central kpc? We will clarify this point in Sect. 5.1. Here instead we go on with another important result:

$$\lambda_c(R_{\text{min1}}) \approx R_{\text{NS}}, R_{\text{NB}}; \quad (7)$$

$$\lambda_c(R_{\text{min2}}) \approx \frac{1}{4} R_{\text{SB}}. \quad (8)$$

Note that $\lambda_c(R)$ matches the radial extent of both the nuclear starburst and the nuclear bar, while it is much shorter than the secondary bar. This result indicates that the nuclear structures of NGC 6946 are intimately related and were most likely generated by the same process of local gravitational instability in the disc, while the strong secondary bar has grown significantly after the onset of instability or was generated by larger-scale processes.

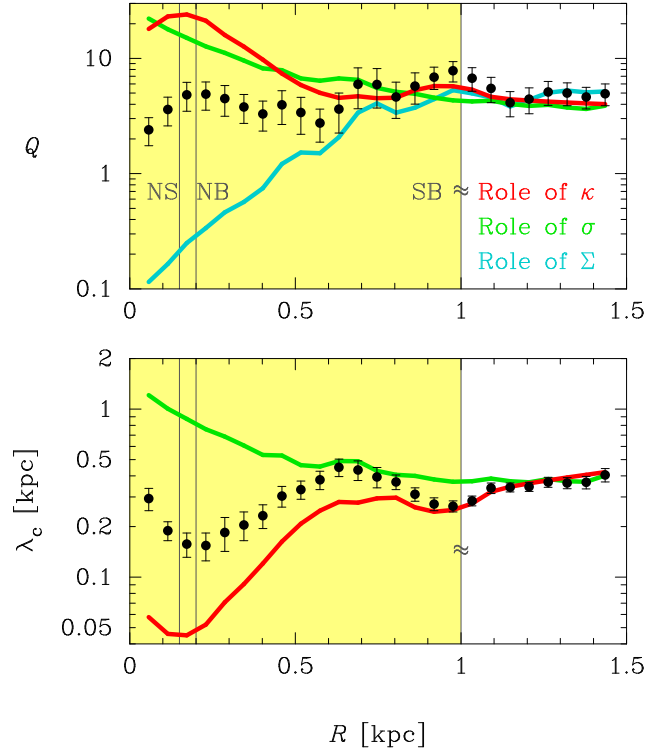


Figure 5. Radial profiles of the Q stability parameter (top) and characteristic instability wavelength (bottom) in the inner region of NGC 6946. The thick lines show the roles of κ , σ and Σ in driving the radial variations of Q and λ_c . The thin lines represent the approximate radial extent of the nuclear starburst (NS), nuclear bar (NB) and secondary bar (SB).

5 DISCUSSION

5.1 What drives the radial variations of Q and λ_c in the central kpc?

In this section, we clarify which physical processes drive the radial variations of Q and λ_c in the central kpc of NGC 6946. For this purpose, we need to understand in more detail how κ , σ and Σ contribute to such variations. We can easily highlight the contribution of, e.g., κ by replacing (σ, Σ) with $(\sigma_{\text{fit}}, \Sigma_{\text{fit}})$ in Eqs (3) and (4), where $\sigma_{\text{fit}}(R)$ and $\Sigma_{\text{fit}}(R)$ are specified in items (ii) and (iii) of Sect. 4.1. Remember, in fact, that using these fits for $R < 1$ kpc suppresses the fundamental differences (in σ and Σ) between the central kpc and the rest of the disc. The contributions of σ and Σ can be highlighted in a similar way.

Fig. 5 shows the contributions defined above (thick lines), together with the original radial profiles of Q and λ_c . The top panel illustrates that κ and Σ play a more significant role than σ in driving the *radial variation* of Q : κ gives rise to the maximum at $R \approx 150\text{--}200$ pc, while Σ contributes to the fluctuations at larger radii. On the other hand, σ has a significant impact on the *magnitude* of Q : it helps κ to counteract the strongly destabilizing effect of Σ , hence to flatten $Q(R)$. The bottom panel illustrates that κ shapes the radial profile of λ_c more faithfully than that of Q . However, even in this case, σ has a strong impact on the magnitude of λ_c . In fact, look at the lower curve. Its minimum at $R \approx 150\text{--}200$ pc is 4 times deeper than that of $\lambda_c(R)$. This means that ignoring the increase of σ towards

the centre, i.e. assuming that $\sigma \approx 10 \text{ km s}^{-1}$ for all R , would underpredict the size of the nuclear starburst and bar by as much as a factor of 4.

The bottom line is that radial inflow (as characterized by κ and Σ) is the main driver for the radial variations of \mathcal{Q} and λ_c in the central kpc. Nevertheless, disc heating (as characterized by σ) is of fundamental importance for flattening the stability level of the disc and for regulating the size of the nuclear structures.

5.2 Is \mathcal{Q} really so large?

In this section, we discuss the physical factors that can push the value of \mathcal{Q} down, closer to unity. To estimate the magnitude of such effects and impose tighter constraints on the stability level of NGC 6946, we need a more general Toomre-like parameter. Romeo & Wiegert (2011) introduced a simple and accurate approximation for the two-component (stars+gas) Q parameter, which takes into account the stabilizing effect of disc thickness and predicts whether the local stability level is dominated by stars or gas. Romeo & Falstad (2013) generalized this approximation to discs made of several stellar and/or gaseous components, and to the whole range of velocity dispersion anisotropy (σ_z/σ_R) observed in galactic discs. In the two-component case, the Q stability parameter is given by

$$\frac{1}{\mathcal{Q}} = \begin{cases} \frac{W}{T_1 Q_1} + \frac{1}{T_2 Q_2} & \text{if } T_1 Q_1 \geq T_2 Q_2, \\ \frac{1}{T_1 Q_1} + \frac{W}{T_2 Q_2} & \text{if } T_2 Q_2 \geq T_1 Q_1, \end{cases} \quad (9)$$

where $Q_i = \kappa \sigma_i / \pi G \Sigma_i$ is the Toomre parameter of component i , σ denotes the radial velocity dispersion, and T_i and W are given by

$$T_i \approx \begin{cases} 1 + 0.6 \left(\frac{\sigma_z}{\sigma_R} \right)_i^2 & \text{for } 0 \lesssim (\sigma_z/\sigma_R)_i \lesssim 0.5, \\ 0.8 + 0.7 \left(\frac{\sigma_z}{\sigma_R} \right)_i & \text{for } 0.5 \lesssim (\sigma_z/\sigma_R)_i \lesssim 1, \end{cases} \quad (10)$$

$$W = \frac{2\sigma_1\sigma_2}{\sigma_1^2 + \sigma_2^2}. \quad (11)$$

This set of equations tells us that the local stability level of the disc is dominated by the component with smaller TQ . The contribution of the other component is suppressed by the W factor. Note, in particular, that if $i = 1$ is the dominant component and σ_1 differs significantly from σ_2 , then $\mathcal{Q} \approx T_1 Q_1$ (as in the one-component case). We are now ready to discuss the physical factors that can push the disc of NGC 6946 closer to marginal instability.

(i) *Stars.* The condition that \mathcal{Q} is dominated by stars (\star) rather than molecular gas (co), $T_\star Q_\star < T_{\text{co}} Q_{\text{co}}$, can be written as

$$\sigma_\star < \sigma_{\text{co}} \left(\frac{\Sigma_\star}{\Sigma_{\text{co}}} \right) \left(\frac{T_{\text{co}}}{T_\star} \right). \quad (12)$$

Gerssen & Shapiro Griffin (2012) showed that $(\sigma_z/\sigma_R)_\star$ decreases markedly from early- to late-type spirals. For an Sc galaxy like NGC 6946, their best-fitting model yields $(\sigma_z/\sigma_R)_\star \approx 0.4$ (see their fig. 4). Hence $T_\star \approx 1.1$. If gas is collisional, as is generally assumed, then $(\sigma_z/\sigma_R)_{\text{co}} \approx 1$ and

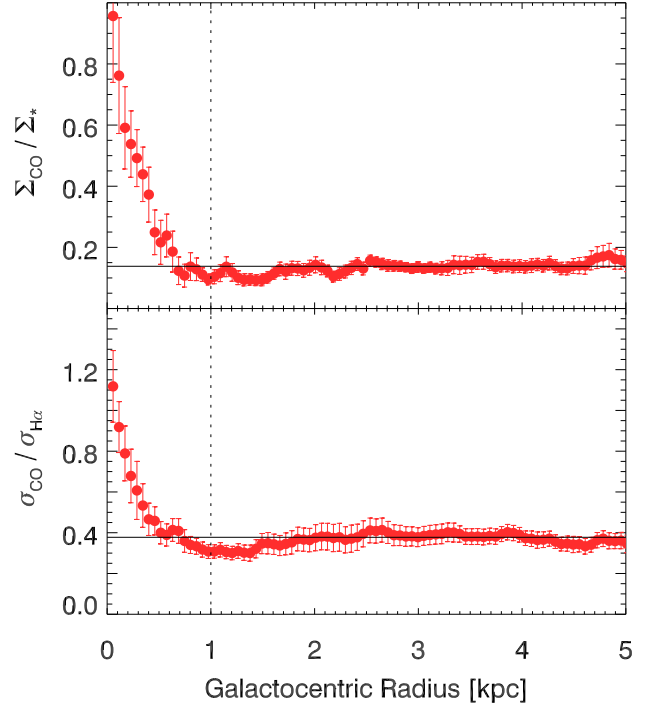


Figure 6. Radial profiles of the ratios between the surface densities of molecular gas and stars (top) and the 1D velocity dispersions of molecular and ionized gas (bottom) in NGC 6946. The solid lines are the median values of $\Sigma_{\text{co}}/\Sigma_\star$ (≈ 0.14) and $\sigma_{\text{co}}/\sigma_{\text{H}\alpha}$ (≈ 0.38) for $R \leq 5$ kpc.

$T_{\text{co}} \approx 1.5$ (see Sect. 4.2). To estimate $\Sigma_\star/\Sigma_{\text{co}}$, we retrieve the Spitzer IRAC 3.6 μm image observed by the SINGS team (Kennicutt et al. 2003), and derive the radial profile of Σ_\star using the same method as for Σ_{co} (see Sect. 3.2) and adopting a fixed K -band mass-to-light ratio, $\Upsilon_\star^K = 0.5 M_\odot/L_{\odot,K}$ (Leroy et al. 2008). The top panel of Fig. 6 illustrates that $\Sigma_\star/\Sigma_{\text{co}} \approx 7$ for $R \gtrsim 1$ kpc, which means that beyond the central kpc the stellar and molecular discs have approximately the same scale length.³ Remembering that $\sigma_{\text{co}} \approx 10 \text{ km s}^{-1}$ for $R \gtrsim 1$ kpc (see Fig. 3), the condition that stars dominate over molecular gas finally becomes $\sigma_\star \lesssim 100 \text{ km s}^{-1}$. Since there are no stellar spectra available for NGC 6946, we check this condition against the model-based radial profile of σ_\star proposed by Leroy et al. (2008). We find that $\sigma_\star \lesssim 100 \text{ km s}^{-1}$ for $R \gtrsim 2$ kpc, therefore stars can actually dominate the value of \mathcal{Q} . But this is not the end of the story. To push the value of \mathcal{Q} down, from $T_{\text{co}} Q_{\text{co}} \approx 4\text{--}5$ to $T_\star Q_\star \approx 1$, we should have $\sigma_\star \approx 20 \text{ km s}^{-1}$, which is true only at the edge of the optical disc: $R \approx 11$ kpc. Even a value of $\mathcal{Q} \approx 2$ would require $\sigma_\star \approx 40\text{--}50 \text{ km s}^{-1}$ and occur at $R \approx 7$ kpc, i.e. still beyond the radial range of our analysis. Thus stars alone cannot solve the problem, unless the model proposed by Leroy et al. (2008) overestimates the real $\sigma_\star(R)$ in NGC 6946. This underlines the importance of

³ Leroy et al. (2008) found that the stellar disc scale length is 30% larger than the molecular one, but again their exponential fits extend over the central kpc, which is physically distinct from the rest of the disc.

having observed, rather than model-based, radial profiles of σ_* when analysing the stability of disc galaxies.

(ii) *Atomic gas.* Detailed comparative analyses of atomic and molecular gas in NGC 6946 show that $\Sigma_{\text{HI}} \ll \Sigma_{\text{CO}}$ for $R \leq 5$ kpc (see fig. 40 of Leroy et al. 2008), while $\sigma_{\text{HI}} \approx \sigma_{\text{CO}}$ (see fig. 4 of Caldú-Primo et al. 2013). As $T_{\text{HI}} \approx T_{\text{CO}} (\approx 1.5)$, this implies that $T_{\text{HI}} Q_{\text{HI}} \gg T_{\text{CO}} Q_{\text{CO}}$ for $R \leq 5$ kpc, i.e. atomic gas cannot dominate the value of Q within the radial range of our analysis.

(iii) *CO-dark molecular gas.* There is growing evidence that a large fraction of molecular gas in the Milky Way is dark, i.e. not traced by CO emission: $M_{\text{dark}} \approx 0.4\text{--}1.6 M_{\text{CO}}$ (e.g., Paradis et al. 2012; Pineda et al. 2013; Kamenetzky et al. 2014; Langer et al. 2014; Smith et al. 2014 and references therein; Chen et al. 2015). Can CO-dark molecular gas play a significant role in the stability scenario of NGC 6946? To answer this question, we need at least rough estimates of both Σ_{dark} and σ_{dark} . We estimate Σ_{dark} from the mass fraction found in the Milky Way: $\Sigma_{\text{dark}} \sim 0.4\text{--}1.6 \Sigma_{\text{CO}}$. The investigations above also suggest that dark molecular gas is warmer and more diffuse than the component traced by CO emission. So σ_{dark} must be bound by $\sigma_{\text{CO}} (\approx \sigma_{\text{HI}})$ and the 1D velocity dispersion of ionized gas: $\sigma_{\text{CO}} \lesssim \sigma_{\text{dark}} \lesssim \sigma_{\text{H}\alpha}$. We derive the radial profile of $\sigma_{\text{H}\alpha}$ from the Fabry-Perot observations of NGC 6946 presented by Fathi et al. (2007), following the same method as for σ_{CO} (see Sect. 3.2). The bottom panel of Fig. 6 illustrates that $\sigma_{\text{H}\alpha} \approx 2.6 \sigma_{\text{CO}}$ for $R \gtrsim 1$ kpc, while $\sigma_{\text{H}\alpha}$ approaches σ_{CO} towards the centre.⁴ Hence $\sigma_{\text{CO}} \lesssim \sigma_{\text{dark}} \lesssim 2.6 \sigma_{\text{CO}}$. As $T_{\text{dark}} \approx T_{\text{CO}} (\approx 1.5)$, we find that $T_{\text{dark}} Q_{\text{dark}} \sim 0.6\text{--}7 T_{\text{CO}} Q_{\text{CO}}$. This means that CO-dark molecular gas can dominate the value of Q and reduce it by more than 40%, but only if $\sigma_{\text{dark}} \sim \sigma_{\text{CO}}$ and $\Sigma_{\text{dark}} \sim 1.6 \Sigma_{\text{CO}}$, the upper bound observed in the Milky Way (Paradis et al. 2012).

(iv) *Anisotropy of the gas velocity dispersion.* As noted in Sect. 4.2, interstellar gas is generally regarded as a collisional component, so that $(\sigma_z/\sigma_R)_{\text{gas}} \approx 1$ and $T_{\text{gas}} \approx 1.5$. Bournaud et al. (2010) analysed the gas velocity field in high-resolution simulations of gas-rich galaxies, and found that the velocity dispersion is isotropic only at scales smaller than the disc scale height. Agertz et al. (2009) showed that at scales of a few 100 pc the gas velocity dispersion has a degree of anisotropy similar to the stellar velocity dispersion. If this is true for NGC 6946, then $(\sigma_z/\sigma_R)_{\text{gas}} \approx 0.4$ and $T_{\text{gas}} \approx 1.1$ [see point (i) above], which implies a 30% reduction in the value of Q .

(v) *Gas turbulence.* Turbulence plays a fundamental role in the dynamics and structure of cold interstellar gas (see, e.g., Agertz et al. 2009; Hennebelle & Falgarone 2012; Falceta-Gonçalves et al. 2014; Roy 2015). The most basic aspect of gas turbulence is the presence of supersonic motions. These are usually taken into account by identifying σ_{gas} with the typical 1D velocity dispersion of the medium, rather than with its thermal sound speed. Another important aspect of gas turbulence is the existence of scaling relations between Σ_{gas} , σ_{gas} and the size of the region over which such quantities are measured (ℓ). Observations show that

$\Sigma_{\text{HI}} \sim \ell^{1/3}$ and $\sigma_{\text{HI}} \sim \ell^{1/3}$ up to scales of 1–10 kpc, whereas $\Sigma_{\text{H}_2} \sim \text{constant}$ and $\sigma_{\text{H}_2} \sim \ell^{1/2}$ up to scales of about 100 pc (see, e.g., Hennebelle & Falgarone 2012; Falceta-Gonçalves et al. 2014; Romeo & Agertz 2014; Roy 2015). Motivated by the large observational uncertainties of $\Sigma_{\text{gas}}(\ell)$ and $\sigma_{\text{gas}}(\ell)$, and having in mind near-future applications to high-redshift galaxies, Romeo et al. (2010) considered more general scaling relations, $\Sigma_{\text{gas}} \propto \ell^a$ and $\sigma_{\text{gas}} \propto \ell^b$, and explored the effect of turbulence on the gravitational instability of gas discs. They showed that turbulence excites a rich variety of stability regimes, several of which have no classical counterpart. See in particular the ‘stability map of turbulence’ (fig. 1 of Romeo et al. 2010), which illustrates such stability regimes and populates them with observations, simulations and models of gas turbulence. Hoffmann & Romeo (2012) extended this investigation to two-component discs of stars and gas, and analysed the stability of THINGS spirals. They showed that gas turbulence alters the condition for star-gas decoupling and increases the least stable wavelength, but hardly modifies the Q parameter at scales larger than about 100 pc. Such predictions have now been confirmed and strengthened by the simulation work of Agertz et al. (2015).

(vi) *Non-axisymmetric perturbations.* Like the original Toomre parameter, Q measures the stability of the disc against local axisymmetric perturbations, so it assumes that $kR \gg 1$. Here the relevant k is the characteristic instability wavenumber, $k_c = 2\pi/\lambda_c$, so the condition $kR \gg 1$ can be written as $\lambda_c \ll 2\pi R$, which is easy to check (see Fig. 4). While this short-wavelength approximation is satisfied by most spiral galaxies (Romeo & Falstad 2013), the assumption of axisymmetric (or tightly wound) perturbations is not so general. Local non-axisymmetric stability criteria are far more complex than Toomre’s criterion: they depend critically on how tightly wound the perturbations are, and cannot generally be expressed in terms of a single effective Q parameter (e.g., Lau & Bertin 1978; Morozov & Khoperskov 1986; Bertin et al. 1989; Jog 1992; Lou & Fan 1998; Griv & Gedalin 2012). However, there is a general consensus that non-axisymmetric perturbations have a destabilizing effect, i.e. a disc with $1 \leq Q < Q_{\text{crit}}$ is still locally unstable against such perturbations. Griv & Gedalin (2012) found that the usual estimate $Q_{\text{crit}} \approx 2$ (see, e.g., Binney & Tremaine 2008) is a real upper limit on the critical stability level. This implies that non-axisymmetric perturbations reduce the value of Q by a factor $1/Q_{\text{crit}} \ll 1/2$, i.e. by much less than 50%. It is highly non-trivial to constrain the magnitude of this effect more tightly than so. The estimates presented in the literature (see references above) depend critically not only on how open the spiral perturbations are, but also on the mathematical treatment of the problem. Tighter constraints on the relative importance of non-axisymmetric and axisymmetric perturbations in spiral galaxies might be found by analysing the radial profile of Q for a large galaxy sample, and by searching for trends in $Q(R)$ along the Hubble sequence. This is however well beyond the scope of the present paper.

The bottom line of this discussion is that stars, CO-dark molecular gas, anisotropy of the gas velocity dispersion and non-axisymmetric perturbations can all play a significant role in the stability scenario of NGC 6946. The disc of NGC

⁴ This result agrees qualitatively with that found by Westfall et al. (2014), namely that $\sigma_{\text{H}\alpha}$ is on average twice as large as σ_{CO} in nearby spiral galaxies.

6946 can indeed be close to marginal instability. Nevertheless, this is most likely the result of all such factors together. None of such factors alone can solve the problem.

Finally, note that the points discussed in this section complement, *but do not invalidate*, the simple and predictive stability analysis carried out in Sect. 4.2. In particular, the radial profile of \mathcal{Q} remains remarkably flat. This is because the main effect here is a systematic reduction in the value of \mathcal{Q} by a factor of order unity. The radial variation of \mathcal{Q} is less significantly affected, so it is still much weaker than that of Σ , κ or σ .

6 CONCLUSIONS

In this paper, we have provided strong evidence that NGC 6946 has a double (nuclear+main) molecular disc, with a clear transition at $R \sim 1$ kpc. We have analysed the disc structure and stability in detail, using robust statistics as well as reliable and predictive diagnostics. Our major conclusions are pointed out below.

- The nuclear molecular disc is exponential, and has central surface density $\Sigma_1 \simeq 2700 \text{ M}_\odot \text{ pc}^{-2}$ and scale length $R_1 \simeq 190$ pc. This is also the approximate radial extent of the nuclear bar. The 1D velocity dispersion decreases steeply from about 50 km s^{-1} at the galaxy centre to about 10 km s^{-1} at the outskirts of the disc, i.e. at a distance of about 1 kpc. The central 1D velocity dispersion is consistent with a disc of moderate thickness, given that the central scale height is a few tens of parsecs, i.e. an order of magnitude smaller than the size of the disc (see Sect. 4.1).

- The main molecular disc is also exponential, and has central surface density $\Sigma_2 \simeq 66 \text{ M}_\odot \text{ pc}^{-2}$ and scale length $R_2 \simeq 2.9$ kpc. Note that Σ_2 is an extrapolated value, since the main and the nuclear discs join at a distance of about 1 kpc. More precisely, the transition in surface density occurs at $R = R_{\text{break}} \simeq 0.75$ kpc and $\Sigma = \Sigma_{\text{break}} \simeq 50 \text{ M}_\odot \text{ pc}^{-2}$. The 1D velocity dispersion is approximately constant up to the outermost radius of the analysis presented here (5 kpc), and has a value of about 10 km s^{-1} .

- These facts imply that the inner region of NGC 6946 is physically distinct from the rest of the disc, and that radial inflow and disc heating have both played a primary role in shaping the central kpc. This is consistent with the fact that the dynamics of NGC 6946 is driven by three bars, and that the strong secondary bar extends up to $R \sim 1$ kpc. It is also consistent with the classical scenario of secular evolution in disc galaxies (see, e.g., Kormendy & Kennicutt 2004; Kormendy 2013; Sellwood 2014).

- The radial profile of the \mathcal{Q} stability parameter is remarkably flat. In spite of the fact that $\Sigma(R)$, $\kappa(R)$ and $\sigma(R)$ exhibit order-of-magnitude variations, $\mathcal{Q}(R)$ fluctuates around a constant value, deviating from it by less than a factor of two! This is an eloquent example of self-regulation: the disc of NGC 6946 is driven by processes that keep it at a fairly constant stability level, except in the central kpc, where the value of \mathcal{Q} is modulated by the nuclear starburst and inner bar within bar. The fact that \mathcal{Q} is well above unity, and on average 4–5, is far more intriguing. We have discussed this issue in great detail and shown that the disc of NGC 6946 can indeed be close to marginal instability, but as a result of four destabilizing factors: stars, CO-dark

molecular gas, anisotropy of the gas velocity dispersion and non-axisymmetric perturbations.

- The radial profile of the characteristic instability wavelength, $\lambda_c(R)$, is a powerful diagnostic that accurately predicts the sizes of starbursts and bars within bars. Such a profile indicates that the nuclear starburst and the nuclear bar of NGC 6946 are intimately related, and were most likely generated by the same process of local gravitational instability in the disc, while the strong secondary bar has grown significantly after the onset of instability or was generated by larger-scale processes.

ACKNOWLEDGMENTS

This work made use of data from the following surveys: BIMA SONG, ‘The BIMA Survey of Nearby Galaxies’ (Helfer et al. 2003); HERACLES, ‘The HERA CO-Line Extragalactic Survey’ (Leroy et al. 2009); and SINGS, ‘The SIRTf Nearby Galaxies Survey’ (Kennicutt et al. 2003). We are very grateful to Oscar Agertz, Guillaume Drouart, Saladin Grebović, John Kormendy, Kirsten Kraiberg Knudsen and Claudia Lagos for useful discussions. We are also grateful to an anonymous referee for constructive comments and suggestions, and for encouraging future work on the topic. KF acknowledges the hospitality of the ESO Garching, where parts of this work were carried out.

REFERENCES

- Agertz O., Lake G., Teyssier R., Moore B., Mayer L., Romeo A. B., 2009, *MNRAS*, 392, 294
- Agertz O., Romeo A. B., Grisdale K., 2015, *MNRAS*, 449, 2156
- Bertin G., Romeo A. B., 1988, *A&A*, 195, 105
- Bertin G., Lin C. C., Lowe S. A., Thurstans R. P., 1989, *ApJ*, 338, 104
- Binney J., Tremaine S., 2008, *Galactic Dynamics*. Princeton University Press, Princeton
- Blasco-Herrera J. et al., 2010, *MNRAS*, 407, 2519
- Boomsma R., 2007, PhD thesis, University of Groningen
- Bournaud F., Elmegreen B. G., Teyssier R., Block D. L., Puerari I., 2010, *MNRAS*, 409, 1088
- Cacciato M., Dekel A., Genel S., 2012, *MNRAS*, 421, 818
- Caldú-Primo A., Schruba A., Walter F., Leroy A., Sandstrom K., de Blok W. J. G., Ianjamasimanana R., Mogotsi K. M., 2013, *AJ*, 146, 150
- Carignan C., Charbonneau P., Boulanger F., Viallefond F., 1990, *A&A*, 234, 43
- Chen B.-Q., Liu X.-W., Yuan H.-B., Huang Y., Xiang M.-S., 2015, *MNRAS*, 448, 2187
- Courteau S., de Jong R. S., Broeils A. H., 1996, *ApJ*, 457, L73
- Daigle O., Carignan C., Amram P., Hernandez O., Chemin L., Balkowski C., Kennicutt R., 2006, *MNRAS*, 367, 469
- Donovan Meyer J. et al., 2012, *ApJ*, 744, 42
- Du M., Shen J., Debattista V. P., 2015, *ApJ*, 804, 139
- Elmegreen B. G., 2011, *ApJ*, 737, 10
- Elmegreen B. G., Elmegreen D. M., Montenegro L., 1992, *ApJS*, 79, 37
- Elmegreen D. M., Chromey F. R., Santos M., 1998, *AJ*, 116, 1221
- Engelbracht C. W., Rieke M. J., Rieke G. H., Latter W. B., 1996, *ApJ*, 467, 227
- Falceta-Gonçalves D., Kowal G., Falgarone E., Chian A. C.-L., 2014, *Nonlin. Processes Geophys.*, 21, 587

- Fathi K., van de Ven G., Peletier R. F., Emsellem E., Falcón-Barroso J., Cappellari M., de Zeeuw T., 2005, *MNRAS*, 364, 773
- Fathi K., Toonen S., Falcón-Barroso J., Beckman J. E., Hernandez O., Daigle O., Carignan C., de Zeeuw T., 2007, *ApJ*, 667, L137
- Fathi K. et al., 2008, *ApJ*, 675, L17
- Fathi K., Beckman J. E., Piñol-Ferrer N., Hernandez O., Martínez-Valpuesta I., Carignan C., 2009, *ApJ*, 704, 1657
- Feigelson E. D., Babu G. J., 2012, *Modern Statistical Methods for Astronomy with R Applications*. Cambridge University Press, Cambridge
- Ferguson A. M. N., Wyse R. F. G., Gallagher J. S., Hunter D. A., 1998, *ApJ*, 506, L19
- Fisher D. B., Drory N., 2008, *AJ*, 136, 773
- Font J., Beckman J. E., Zaragoza-Cardiel J., Fathi K., Epinat B., Amram P., 2014, *MNRAS*, 444, L85
- Forbes J., Krumholz M., Burkert A., 2012, *ApJ*, 754, 48
- Forbes J. C., Krumholz M. R., Burkert A., Dekel A., 2014, *MNRAS*, 438, 1552
- Friedli D., Martinet L., 1993, *A&A*, 277, 27
- Fuchs B., von Linden S., 1998, *MNRAS*, 294, 513
- Gerssen J., Shapiro Griffin K., 2012, *MNRAS*, 423, 2726
- Glover S. C. O., Mac Low M.-M., 2007, *ApJ*, 659, 1317
- Griv E., Gedalin M., 2012, *MNRAS*, 422, 600
- Griv E., Gedalin M., Yuan C., 2002, *A&A*, 383, 338
- Helfer T. T., Thornley M. D., Regan M. W., Wong T., Sheth K., Vogel S. N., Blitz L., Bock D. C.-J., 2003, *ApJS*, 145, 259
- Hennebelle P., Falgarone E., 2012, *A&ARv*, 20, 55
- Hernandez O., Wozniak H., Carignan C., Amram P., Chemin L., Daigle O., 2005, *ApJ*, 632, 253
- Ho L. C., Greene J. E., Filippenko A. V., Sargent W. L. W., 2009, *ApJS*, 183, 1
- Hoffmann V., Romeo A. B., 2012, *MNRAS*, 425, 1511
- Huber P. J., Ronchetti E. M., 2009, *Robust Statistics*. Wiley, Hoboken
- Jog C. J., 1992, *ApJ*, 390, 378
- Kamenetzky J., Rangwala N., Glenn J., Maloney P. R., Conley A., 2014, *ApJ*, 795, 174
- Kennicutt R. C. Jr., 1989, *ApJ*, 344, 685
- Kennicutt R. C. Jr. et al., 2003, *PASP*, 115, 928
- Kormendy J., 2013, in Falcón-Barroso J., Knapen J. H., eds, *Secular Evolution of Galaxies*. Cambridge University Press, Cambridge, p. 1
- Kormendy J., Kennicutt R. C. Jr., 2004, *ARA&A*, 42, 603
- Kormendy J., Drory N., Bender R., Cornell M. E., 2010, *ApJ*, 723, 54
- Krumholz M., Burkert A., 2010, *ApJ*, 724, 895
- Langer W. D., Velusamy T., Pineda J. L., Willacy K., Goldsmith P. F., 2014, *A&A*, 561, A122
- Lau Y. Y., Bertin G., 1978, *ApJ*, 226, 508
- Leroy A. K., Walter F., Brinks E., Bigiel F., de Blok W. J. G., Madore B., Thornley M. D., 2008, *AJ*, 136, 2782
- Leroy A. K. et al., 2009, *AJ*, 137, 4670
- Lindblad P. O., 1960, *Stockholms Obser. Ann.*, 21, 4
- Lou Y.-Q., Fan Z., 1998, *MNRAS*, 297, 84
- MacArthur L. A., Courteau S., Holtzman J. A., 2003, *ApJ*, 582, 689
- Mac Low M.-M., Klessen R. S., 2004, *Rev. Mod. Phys.*, 76, 125
- Martig M., Minchev I., Flynn C., 2014, *MNRAS*, 443, 2452
- Martin C. L., Kennicutt R. C. Jr., 2001, *ApJ*, 555, 301
- Morozov A. G., Khoperskov A. V., 1986, *Ap*, 24, 266
- Müller J. W., 2000, *J. Res. Natl. Inst. Stand. Technol.*, 105, 551
- Paradis D., Dobashi K., Shimoikura T., Kawamura A., Onishi T., Fukui Y., Bernard J.-P., 2012, *A&A*, 543, A103
- Pineda J. L., Langer W. D., Velusamy T., Goldsmith P. F., 2013, *A&A*, 554, A103
- Rautiainen P., Salo H., Laurikainen E., 2002, *MNRAS*, 337, 1233
- Regan M. W., Vogel S. N., 1995, *ApJ*, 452, L21
- Regan M. W., Thornley M. D., Helfer T. T., Sheth K., Wong T., Vogel S. N., Blitz L., Bock D. C.-J., 2001, *ApJ*, 561, 218
- Renaud F. et al., 2013, *MNRAS*, 436, 1836
- Romeo A. B., 1990, *Stability and Secular Heating of Galactic Discs*. PhD thesis, SISSA, Trieste, Italy
- Romeo A. B., Agertz O., 2014, *MNRAS*, 442, 1230
- Romeo A. B., Falstad N., 2013, *MNRAS*, 433, 1389
- Romeo A. B., Wiegert J., 2011, *MNRAS*, 416, 1191
- Romeo A. B., Horellou C., Bergh J., 2003, *MNRAS*, 342, 337
- Romeo A. B., Horellou C., Bergh J., 2004, *MNRAS*, 354, 1208
- Romeo A. B., Burkert A., Agertz O., 2010, *MNRAS*, 407, 1223
- Rousseeuw P. J., 1991, *J. Chemometrics*, 5, 1
- Roy N., 2015, preprint (arXiv:1502.01022)
- Schinnerer E., Böker T., Emsellem E., Lisenfeld U., 2006, *ApJ*, 649, 181
- Schinnerer E., Böker T., Emsellem E., Downes D., 2007, *A&A*, 462, L27
- Schoenmakers R. H. M., Franx M., de Zeeuw P. T., 1997, *MNRAS*, 292, 349
- Schwarz M. P., 1984, *MNRAS*, 209, 93
- Sellwood J. A., 2014, *Rev. Mod. Phys.*, 86, 1
- Shlosman I., 2002, in Athanassoula E., Bosma A., Mujica R., eds, *ASP Conf. Ser. Vol. 275, Disks of Galaxies: Kinematics, Dynamics and Perturbations*. Astron. Soc. Pac., San Francisco, p. 231
- Shlosman I., Frank J., Begelman M. C., 1989, *Nature*, 338, 45
- Smith R. J., Glover S. C. O., Clark P. C., Klessen R. S., Springel V., 2014, *MNRAS*, 441, 1628
- Tasker E. J., 2011, *ApJ*, 730, 11
- Toomre A., 1964, *ApJ*, 139, 1217
- Tsai C.-W., Turner J. L., Beck S. C., Meier D. S., Wright S. A., 2013, *ApJ*, 776, 70
- van der Kruit P. C., Freeman K. C., 2011, *ARA&A*, 49, 301
- Walsh W., Beck R., Thuma G., Weiss A., Wielebinski R., Dumke M., 2002, *A&A*, 388, 7
- Westfall K. B., Andersen D. R., Bershady M. A., Martinsson T. P. K., Swaters R. A., Verheijen M. A. W., 2014, *ApJ*, 785, 43
- Wilson C. D. et al., 2011, *MNRAS*, 410, 1409
- Wong T., Blitz L., Bosma A., 2004, *ApJ*, 605, 183
- Wozniak H., 2015, *A&A*, 575, A7
- Zhang X., 1998, *ApJ*, 499, 93
- Zimmer P., Rand R. J., McGraw J. T., 2004, *ApJ*, 607, 285

This paper has been typeset from a $\text{\TeX}/\text{\LaTeX}$ file prepared by the author.